

LARGE EDDY SIMULATION OF SEPARATED FLOW IN A STREAMWISE PERIODIC CHANNEL CONSTRICTION

Lionel Temmerman and Michael A. Leschziner

Department of Aeronautics

Imperial College of Science, Technology and Medicine

Prince Consort Rd.

London SW7 2BY, UK

l.temmerman@ic.ac.uk, mike.leschziner@ic.ac.uk

ABSTRACT

The ability of LES to resolve separation from the leeward side of a curved "hill" in a periodically constricted channel is investigated. The emphasis is on the effectiveness of different combinations of subgrid-scale models and wall-functions used on relatively coarse grids. Accuracy is judged by reference to a highly-resolved simulation on a $4.6 \cdot 10^6$ nodes grid, allowing Reynolds-stress budgets, realisability and structural features to be analysed. It is demonstrated that even gross-flow parameters, such as separation-bubble length, are very sensitive to modelling approximations and grid quality.

INTRODUCTION

LES is highly effective for resolving flows which are dominated by free shear layers separating at sharp edges and governed, predominantly, by large-scale structures. In contrast, flows for which the gross flow features are materially affected by viscous near-wall processes pose a major challenge to LES, especially at high Reynolds numbers. Near a wall, LES is required, in effect, to approach DNS, as the dynamically important scales diminish rapidly towards the dissipative ones, and turbulence approaches a two-component state. This behaviour has important implications in respect of grid density and quality, resource-requirements and near-wall representation of subgrid-scale transport and dissipation.

The above issues are especially pertinent to flows in which separation is provoked on a gently curved or sloping wall by the sustained action of an adverse pressure gradient on the decelerating boundary layer - for example, on a highly-loaded aerofoil or blade. The structure of such a boundary layer will influence the separation line, both instantaneous

and time-averaged. At the high Reynolds numbers encountered in practical applications, the resource requirements of a wall-resolved simulation quickly become prohibitive, and economical compromises must be sought.

One such compromise is to bridge the semi-viscous near-wall layer by a "wall-function", based on an assumed shape for the instantaneous velocity between the nodes closest to the wall and the wall itself. Variants include a power-law profile (Werner and Wengle, 1991) and the log-law profile (Grötzbach, 1987). Both are designed to return an estimate of the instantaneous wall shear stress for a given velocity at the wall-nearest node, which then serves as a wall boundary condition for the outer LES domain. While wall-functions have been used extensively in flows which are largely unaffected by boundary-layer details, little is known about their effectiveness in attached as well as separated flows in which near-wall processes are expected to be highly influential. Other, more elaborate approaches rest on matching RANS-type near-wall models, based on conventional statistical closures, to the outer LES domain. Variants include the two-layer approach of Balaras et al (1996), recently investigated by Cabot and Moin (1999) for a separated backward-facing-step flow, and the "Detached Eddy Simulation" strategy of Spalart et al (1997).

This paper investigates the effectiveness of different combinations of SGS models and wall-functions in simulating separation from a curved surface. The geometry, shown in Fig. 1, is a streamwise-periodic, spanwise-homogeneous channel segment with one wall containing hill-shaped constrictions, 9 hill heights apart. The Reynolds number is 10595. This is a modification of an experimental configuration examined by Almeida et al (1993), motivated by a combination of cost consid-

erations and the observation that the experimental flow was not fully periodic, that spanwise confinement provokes spanwise variations, and that the short distance between consecutive hills did not permit a significant post-reattachment recovery region to be established prior to the acceleration of the flow by the following hill. The flow offers the important advantage of not requiring boundary conditions, except for those at the two walls. The assessment of alternative wall-function implementations is based on data derived from two highly-resolved simulations, using the same grid of $4.6 \cdot 10^6$ nodes, in which the SGS viscosity is of order of the fluid viscosity. The two simulations were performed with two entirely different codes, one by Mellen et al (2000) and the other by the authors. Here, the simulation data are used, in effect, in lieu of experimental data to investigate sensitivity to SGS modelling, grid density and approximate near-wall treatments.

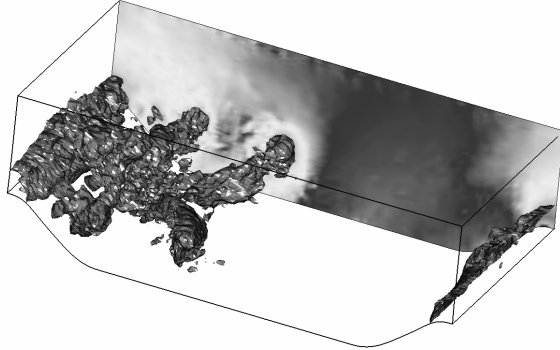


Figure 1: Constricted channel geometry with instantaneous pressure isosurfaces.

NEAR-WALL TREATMENT

Four different formulations have been investigated, three utilising different forms of the log-law and the fourth a power-law approximation. The simplest (LL2) is based on the assumption that the near-wall layer consists (in an instantaneous sense) of a fully viscous sublayer and a fully turbulent layer with the interface at $y^+ \leq 11$:

$$u^+ = y^+ \quad if \quad y^+ \leq 11 \quad (1)$$

$$u^+ = \frac{1}{\kappa} \ln(Ey^+) \quad if \quad y^+ > 11 \quad (2)$$

A three-layer generalisation (LL3) of the above form accounts for the buffer region which is described by a modified log-function fit (Dahlström and Davidson, 2000) as follows:

$$u^+ = y^+ \quad if \quad y^+ \leq 11 \quad (3)$$

$$u^+ = A \ln(y^+) + B \quad if \quad 5 < y^+ \leq 30 \quad (4)$$

$$u^+ = \frac{1}{\kappa} \ln(Ey^+) \quad if \quad y^+ > 30 \quad (5)$$

with $A = (\frac{1}{\kappa} \ln(30E) - 5)/\ln(6)$ and $B = 5 - A \ln(5)$.

In the above near-wall approximations, the velocity scale in y^+ is formed with the wall shear stress, restricting their validity, in a statistical sense, to the state of turbulence-energy equilibrium. In RANS computations, the applicability of the log-law may be extended considerably by using the turbulent energy to scale y , a substitution based on the equivalence $u_\tau^2 = C_\mu^{0.5} k$. This concept may also be applied to LES (Murakami et al, 1993), with k chosen to be the resolved turbulent energy at the wall-nearest node. Thus, the universal wall distance becomes:

$$y^+ = \frac{y C_\mu^{1/4} k^{1/2}}{\nu} \quad (6)$$

Otherwise, the wall-law (LLK) is identical to the first form, eqs. (1) and (2).

The fourth variant (WW) is a simplification of the two-layer log-law form proposed by Werner and Wengle (1991). This is based on an explicit power-law approximation to the log-law outside the viscous sublayer, interfaced with the linear profile in the viscous sublayer:

$$u^+ = y^+ \quad if \quad y^+ \leq 11.8 \quad (7)$$

$$u^+ = 8.3 (y^+)^{\frac{1}{7}} \quad if \quad y^+ > 11.8 \quad (8)$$

SUBGRID-SCALE MODELLING

SGS models considered here are all based on the eddy-viscosity concept,

$$\tau_{ij} - \frac{\delta_{ij}}{3} \tau_{kk} = -2\nu_t \bar{S}_{ij} \quad (9)$$

Simulations have been performed with the SGS models given in Table 1. A detailed exposition of the above models is not possible here, but a few clarifying comments are given below.

The basic Smagorinsky model (SMAG) is used in conjunction with the van Driest damping functions (WF1, WF2) which ensure that the SGS viscosity vanishes as the wall is approached. The difference between variants WF1 and WF2 lies in the value of A^+ .

The dynamic Smagorinsky model (DYN) is that proposed by Germano et al (1991) and modified by Lilly (1992). Test-filtering is performed in the streamwise-spanwise grid planes.

Model Designation	Model Description
SMAG	Smagorinsky ($C_s = 0.1$)
SMAG + WF1	Smagorinsky ($C_s = 0.1$) wall-damping function ($A^+ = 5$)
SMAG + WF2	wall-damping function ($A^+ = 5$) Smagorinsky ($C_s = 0.1$) wall-damping function ($A^+ = 25$)
MSM	Mixed Scale Model
DYN	Dynamic Smagorinsky model
WALE	WALE Model ($C_w = 0.1$)
LDYN	Localised dynamic Smagorinsky model

Table 1: Summary of SGS models used.

Stability is enhanced by spatial averaging over any statistically homogeneous direction and by constraining the SGS viscosity to remain positive.

The localized dynamic Smagorinsky model (LDYN) by Piomelli and Liu (1995) is a variant of the previous model, wherein the dynamic coefficient is allowed to vary during the test-filtering operation. This requires the use of a iterative solver to find the dynamic coefficient at each time-step. Alternatively, the value of this coefficient at the previous time-step can be used as an approximation.

The mixed-scale model (Sagaut, 1996) is based on a weighted geometric average of SGS viscosities in which the velocity scale is related, respectively, to S_{ij} (as done in the Smagorinsky model) and to the SGS turbulence energy \bar{k} , obtained by the application of a test filter analogous to that used for dynamic modelling.

Finally, the WALE model (Nicoud and Ducros, 1999) is specifically designed to return the correct wall asymptotic y^3 variation of the SGS viscosity. It does so by a particular manipulation of the strain tensors and its components within an expression of similar in structure to the Smagorinsky model.

COMPUTATIONAL PROCEDURE

The LES equations are solved using a second-order fractional-step method with a multiblock/multigrid non-orthogonal finite-volume approach with the variables stored at cell centroids. The time derivative is approximated by a second-order backward Euler scheme. Convection and diffusion are approximated by second-order centred interpolation and are advanced in time using the Adams-Bashforth scheme. Pressure is obtained by solving the pressure-Poisson equation using partial diagonalisation in conjunction with a V-cycle multigrid scheme and LSOR relaxation. The code is fully parallelised. Details of the parallel implementation on various architectures and its efficiency can be found in

Temmerman et al (2000).

CHANNEL-FLOW SIMULATIONS

As a precursor to the main study of separated flow, simulations were undertaken for fully-developed channel flow, to investigate the performance of alternative SGS models and examine the ability of the wall laws to return the log-law behaviour with coarse near-wall grids for a Reynolds number that is comparable to that of the hill flow. Simulations were performed for the case $Re_\tau = 590$ for which DNS data by Moser et al (1999) are available for comparison. Most wall-layer-resolving simulations were done on a $96 \times 64 \times 64$ grid, covering a box of $2\pi h \times 2h \times \pi h$ and having cell-aspect ratios $(\Delta x^+, \Delta y^+, \Delta z^+) = (38, 2 - 42, 29)$, the lowest $\Delta y^+ = 2$ being that at the wall. Statistical properties were assembled over a period of 12 flow-through times.

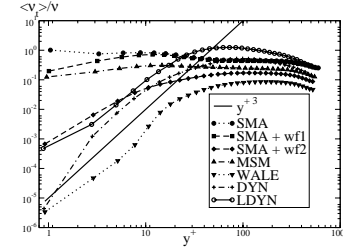


Figure 2: SGS viscosity for channel flow, wall-resolved simulation.

In wall-layer-resolving simulations, the SGS viscosity level in the upper portion of the buffer layer and its asymptotic near-wall behaviour were observed to be particularly influential. Variations of this viscosity are shown in Fig. 2. The only models found to return the theoretical y^{+3} decay reasonably well are the WALE and the dynamic formulations, although the latter gives substantially higher viscosity values away from the wall. Table 2 compares errors in centre-line velocity and wall-shear Reynolds numbers, while Fig. 3 shows the velocity profiles, in wall co-ordinates, and turbulence-intensity profiles obtained with the WALE model, judged to give the best overall behaviour.

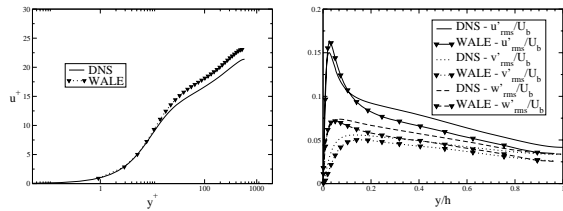


Figure 3: Velocity and turbulence intensities for channel flow, wall-resolved simulation.

SGS Model	Re_τ	Error	u_c/U_b	Error
DNS	584	-	1.1418	-
SMAG	617	+5.6 %	1.1533	+1.00 %
MSM	578	-1.0 %	1.1424	+0.05 %
SMAG & wf1	595	+1.8 %	1.1444	+0.23 %
SMAG & wf2	538	-7.8 %	1.1319	-0.86 %
DYN	529	-9.3 %	1.1298	-1.05 %
WALE	542	-7.1 %	1.1440	+0.20 %
LDYN	520	-10.9 %	1.1221	-1.73 %

Table 2: Wall shear stress and centreline velocity for channel flow, wall-resolved simulation.

SGS Model	Re_τ	Error	u_c/U_b	Error
DNS	584	-	1.1418	-
WALE + LL2	558.5	-4.4 %	1.12	-1.91 %
WALE + LL3	557.8	-4.5 %	1.118	-2.08 %
WALE + LLK	537.6	-7.9 %	1.13	-1.03 %
WALE + WW	598.4	2.5 %	1.133	-0.08 %

Table 3: Wall shear stress and centreline velocity for channel flow, wall-function simulation.

Simulations were then performed with the four wall-laws and the WALE model for $Re_\tau = 590$ over a deliberately coarser grid of $64 \times 32 \times 32$ nodes giving cell-aspect ratios ratios ($\Delta x^+, \Delta y^+, \Delta z^+$) $\approx (58, 37, 58)$. Table 3 compares errors in centre-line velocity and wall-shear Reynolds numbers, while Fig. 4 gives velocity and turbulence-intensity profiles for the four wall-law formulations. The results illustrate that, despite the evidently serious resolution limitations which arise when coarse grids are used, the simulations are able to resolve the essential features of the statistical fields.

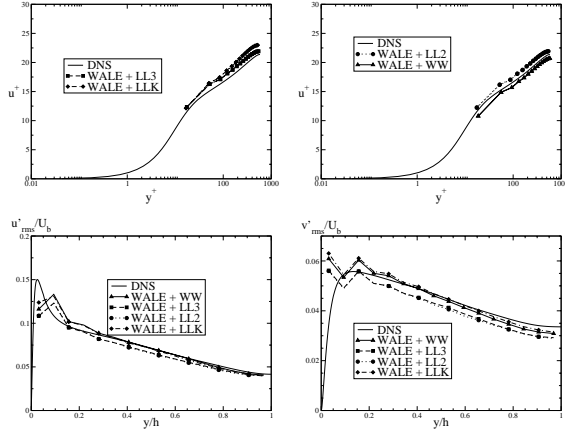


Figure 4: Velocity and turbulence intensities for channel flow, wall-function simulations.

HIGHLY-RESOLVED SIMULATION OF SEPARATED CHANNEL FLOW

To enable the accuracy of coarse-grid/wall-functions simulations to be assessed for the separated flow shown in Fig. 1, a highly-resolved reference simulation was performed over a grid of $4.6 \cdot 10^6$ ($196 \times 128 \times 186$) cells. The channel is $9h$ long, $3.036h$ high and $4.5h$ deep, h being the hill height. The Reynolds

number is 10595. The mesh is close to orthogonal, of low aspect ratio over most of the flow domain and mesh expansion ratio below 1.05. The y^+ -value at the nodes closest to the lower wall is around 0.5. SGS effects are represented by the WALE model, giving viscosity values below that of the fluid viscosity over most of the flow domain. A similar simulation was also performed by Mellen et al (2000), and this gave results in close agreement to the present ones. A few statistical results, derived by integration over 55 through-flow periods, are shown in Figs. 5-8.

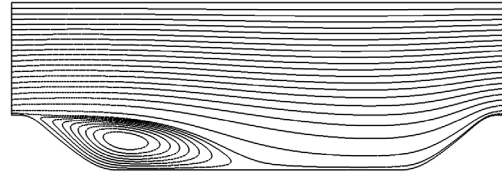


Figure 5: Streamlines for the highly-resolved simulation.

Fig. 5 gives the time-averaged streamfunction field. The flow separates at $x = 0.22h$ and reattaches at $x = 4.72h$. Velocity and normal-stress profiles are included in comparisons to follow in the next section. Adherence to realisability constraints is demonstrated in Fig. 6 which gives 3 cross-flow profiles relating the second and third stress invariants on Lumley's realisability map. The simulation was also used to extract stress budgets, currently employed to examine second-moment closures. Fig. 7 gives the turbulence-energy budget at the location $x = 2h$, midway along the separation bubble. Dissipation was obtained from the balance of other processes. The behaviour across the shear-layer is observed to be qualitatively close to that reported by Le et al (1997) in their DNS of a backward-facing-step flow, while the near-wall behaviour is quite similar to that in an ordinary channel flow (Mansour et al, 1988).

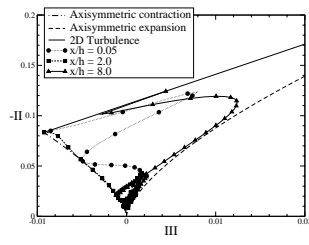


Figure 6: Realisability map for 3 cross-flow traverses.

The simulation allowed *a-priori* testing of the wall-functions to be undertaken. Fig. 8 gives an example in which the Werner-Wengle approximation was used to extract the instantaneous wall-shear stress from the velocity resolved at different distances (grid lines) from

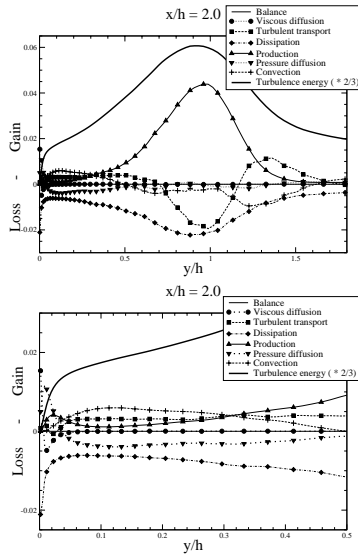


Figure 7: Turbulent-energy budget at $x/h = 2.0$; left: across the shear layer; right: zoom on the lower wall region, highly-resolved simulation.

the wall in the mid-span plane. This test illustrates the smoothing effect of the wall-function treatment and its tendency to seriously underestimate the peak wall-shear stress. These defects reflect, in parts, the fact that the near-wall velocity profiles, shown in Fig. 9 at 3 streamwise locations, do not adhere, either statistically or instantaneously, to the velocity-profile assumptions underpinning the wall laws.

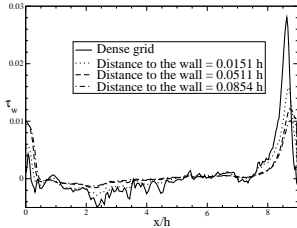


Figure 8: Instantaneous wall-shear stress derived from the Werner-Wengle wall-treatment at 3 grid lines progressively removed from the wall.

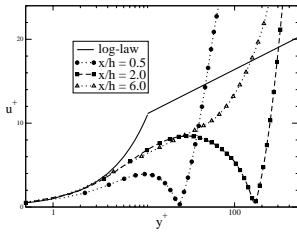


Figure 9: Near-wall velocity profiles at 3 streamwise locations derived from highly-resolved simulation.

WALL-FUNCTION SIMULATIONS OF SEPARATED CHANNEL FLOW

Coarse-grid simulations were performed along three parametric 'axes' - grid density,

Grid $N_x \times N_y \times N_z$	SGS & Wall Model	$(\frac{x}{h})_{sep.}$	$(\frac{x}{h})_{reat.}$
196 × 128 × 186	WALE + NS	0.22	4.72
176 × 64 × 92	WALE + NS	0.38	3.45
176 × 64 × 92	WALE + WW	0.32	4.56
176 × 64 × 92	WALE + LL3	0.34	4.32
112 × 64 × 92	WALE + NS	1.12	2.17
112 × 64 × 92	WALE + WW	0.46	4.00
112 × 64 × 92	WALE + LL2	0.54	2.95
112 × 64 × 92	WALE + LL3	0.53	2.98
112 × 64 × 92	WALE + LLK	0.49	3.38
112 × 64 × 92	SMA & WF2 + WW	0.50	3.59
112 × 64 × 92	MSM + WW	0.45	4.18
112 × 64 × 92	DYN + WW	0.46	3.56
112 × 64 × 92	LDYN + WW	0.47	3.56

Table 4: Separation and reattachment locations for constricted-channel simulations.

SGS modelling and wall-law approximations - to permit an appreciation of the relative importance of the three issues in relation to predictive accuracy.

Table 4 provides a comparison of predicted separation and reattachment positions obtained with different SGS models, wall-functions and grid densities (NS indicates "no-slip" conditions). As seen, both positions are materially sensitive to all three parameters. Especially poor results are obtained when the streamwise grid density is low in the vicinity of the separation point ($112 \times 64 \times 92$ grid) and when the no-slip condition is applied. Reasonably good results are returned by the combination of WALE model and the Werner-Wengle or 3-layer wall law approximation, provided adequate resolution around the separation location.

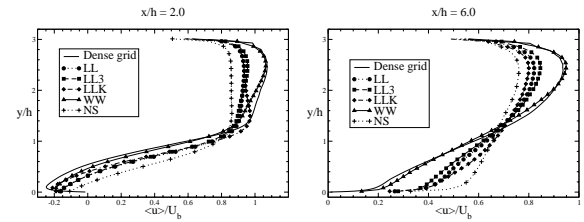


Figure 10: Distribution of streamwise velocity with the WALE model and 4 wall-treatments on the coarsest grid.

Comparisons of streamwise velocity and streamwise stress at two locations, one in the recirculation zone and the other in the post-reattachment recovery region, are given in Figs. 10-12. The velocity profiles (Fig. 10 and 11) were obtained using the coarse and medium grids and the WALE model. Fig. 12 shows the streamwise stresses obtained with the medium grid ($176 \times 64 \times 92$), the WALE model and three wall-treatments.

The results reinforce the observation that substantial errors can arise especially from insufficient resolution around the separation

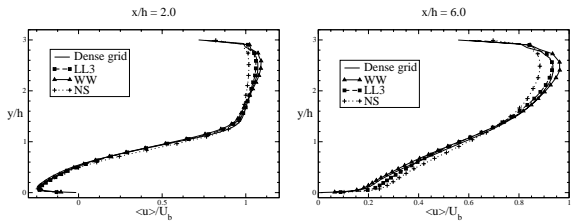


Figure 11: Distribution of streamwise velocity with the WALE model for 3 wall-treatments and the medium grid.

point, in which case, sensitivity to SGS and near-wall modelling is very high. As resolution improves, this sensitivity declines and reasonable agreement with the highly-resolved solution is obtained. Although none of the simulations is satisfactory, those using Werner-Wengle wall-law and the WALE model models are found to give results closest to the highly-resolved simulation.

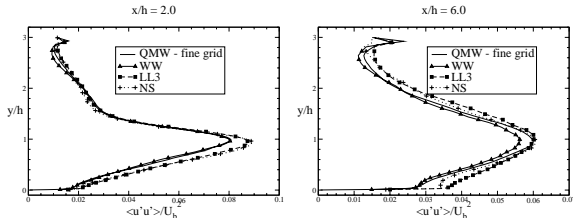


Figure 12: Distribution of streamwise stress with the WALE model for 3 wall-treatments and the medium grid.

CONCLUSIONS

The study has demonstrated that the simulation of separation from curved surfaces can be very sensitive to the grid density, the details of the near-wall treatment and the nature of the SGS model. This sensitivity appears to be rooted, principally, in variations of the predicted separation point: a small downstream shift of this point leads to a major shortening of the recirculation region and major changes in gross flow features. In the present flow, sensitivity seems to be especially pronounced because of the periodic nature of the flow and because the boundary layer is subjected, prior separation, to large rates of streamwise straining, and thus structural changes.

Of the practices examined, the combination of the WALE SGS model, giving low levels of SGS viscosity, and Werner-Wengle near-wall approximation is the most effective in returning the closest fidelity to the highly-resolved solution. *A-priori* tests show that the true near-wall flow does not adhere well to the assumptions underpinning any of the wall-laws used. Thus, better near-wall treatments are imperative if the physical realism of coarse-grid simulations is to be improved.

ACKNOWLEDGMENTS

This work is part of the "LESFOIL" EU-project (No. BRPR-CT97-0565), financed through the Brite-Euram programme.

REFERENCES

- Almeida, G.P., Durão, D.F.G., and Heitor, M.V., 1993, *Experimental Thermal and Fluid Science*, Vol. 7, pp. 87-101.
- Balaras, E., Benocci, C., and Piomelli, U., 1996, *AIAA Journal*, Vol. 34, pp. 1111-1119.
- Cabot, W., and Moin, P., 1999, *Flow, Turbulence and Combustion*, Vol. 63, pp. 269-291.
- Dahlström, S., and Davidson, L., 2000, *Proceedings, ECCOMAS 2000*.
- Germano, M., Piomelli, U., Moin, P., and Cabot, W.H., 1991, *Physics of Fluids A*, Vol. 3 , pp. 1760-1765.
- Grötzschbach, G., 1987, *Encyclopedia of Fluid Mechanics*, Vol. 6, pp. 1337-1391.
- Le, H., Moin, P., and Kim, J., 1997, *Journal of Fluid Mechanics*, Vol. 330, pp. 349-374.
- Lilly, D.K., 1992, *Physics of Fluids A*, Vol. 4, pp. 633-635.
- Mansour, N.N., Kim, J., and Moin, P., 1988, *Journal of Fluid Mechanics*, Vol. 194, pp. 15-44.
- Mellen, C.P., Fröhlich, J., and Rodi, W., 2000, *Proceedings, 16th IMACS World Congress*.
- Moser, R.D., Kim, J and Mansour, N.N, 1999, *Physics of Fluids*, Vol. 11, pp. 943-945.
- Murakami, S., Mochida, A., Rodi, W., and Sakamoto, S., 1993, *ASME FED, Engineering applications of large eddy simulations*, Vol. 162, pp. 113-120.
- Nicoud, F., and Ducros, F., 1999, *Flow, Turbulence and Combustion*, Vol. 62, pp. 183-200.
- Piomelli, U., and Liu, J., 1995, *Physics of Fluids*, Vol. 7, pp. 839-848.
- Sagaut, P., 1996, *La Recherche Aérospatiale*, Vol. 1, pp. 51-63.
- Smagorinsky, J., 1963, *Monthly Weather Review*, Vol. 91, pp. 99-163.
- Spalart, P.R., Jou, W-H., Strelets, M., and Allmaras, S.R., 1997, *Proceedings, Advances in DNS/LES*.
- Temmerman, L., Leschziner, M.A., Ashworth, and Emerson, D.R., 2000, *Proceedings, Parallel CFD 2000*.
- Werner, H., and Wengle, H., 1991, *Proceedings, 8th Symposium on Turbulent Shear Flows*, pp. 155-168.